Cerebral Cortex June 2009;19:1345–1359
doi:10.1093/cercor/bhn175
Advance Access publication October 8, 2008

Two Calretinin-Positive GABAergic Cell Types in Layer 2/3 of the Mouse Neocortex Provide Different Forms of Inhibition

Antonio Caputi[1], Andrei Rozov[1,3], Maria Blatow[2] and Hannah Monyer[1]

[1]Department of Clinical Neurobiology and [2]Department of Neuroradiology, University of Heidelberg, 69120 Heidelberg, Germany
[3]Current address: Neurosciences Institute, Ninewells Hospital and Medical School, University of Dundee, Dundee DD1 9SY, UK. Email: a.rozov@dundee.ac.uk.

The first 2 authors equally contributed to this work.

Calretinin (CR)–positive GABAergic (gamma-aminobutyric acidergic) interneurons have been suggested to target preferentially other GABAergic cells in the neocortex. To systematically study this cell population in the cortex, we generated transgenic mice that express enhanced green fluorescent protein (EGFP) under the control of the CR promoter and characterized EGFP/CR-positive cells at the cellular and network level. Based on anatomical and electrophysiological characteristics, 2 types of EGFP/CR-positive cells could be distinguished that we termed bipolar (BCR) and multipolar (MCR) CR cells. Both cell types share the feature of preferential interneuron targeting but differ in most other characteristics, including firing pattern, biochemical markers, neurite arborization, and synaptic plasticity. Like many other GABAergic interneurons, BCR cells but not MCR cells exhibit restricted cell type-specific gap junction coupling. Notably, MCR cells are electrically coupled in an asymmetric fashion with GABAergic interneurons of another subtype, the parvalbumin-positive multipolar bursting (MB) cells. Most importantly, the strength of electrical coupling between MCR and MB cells underlies their synchronous activation during carbachol-induced oscillations.

Keywords: interneuron, gap junctions, oscillations, parvalbumin, short-term plasticity

Introduction

GABAergic (gamma-aminobutyric acidergic) interneurons represent the epitome of cellular diversity in the neocortex. The classification of these cells has been based on different criteria including anatomical features, neurochemical markers, electrophysiological, or molecular characteristics both in neocortex (DeFelipe 1997; Markram et al. 2004) and hippocampus (Freund and Buzsaki 1996; McBain and Fisahn 2001).

GABAergic interneurons were shown to be critically involved in timing the output of pyramidal cells and hence they play a major role in orchestrating network activity at different frequency ranges in several brain regions, including hippocampus (Cobb et al. 1995; Whittington et al. 1995; Ylinen, Bragin, et al. 1995; Ylinen, Soltesz, et al. 1995; Tamas et al. 2000), neocortex (Buhl et al. 1998; Roopun et al. 2006; Gireesh and Plenz 2008), and entorhinal cortex (Cunningham et al. 2003). Recent elegant in vivo studies provided evidence that the firing of specific interneuron subtypes is phase-locked to defined oscillatory activity thus providing a dynamic, spatio-temporal control of pyramidal cells (Somogyi and Klausberger 2005).

This study focused on a subclass of GABAergic interneurons, the calretinin (CR)–positive interneurons, that, depending on the forebrain region, represent 10–30% of the total GABAergic cell population (Gonchar and Burkhalter 1999). Previous studies indicated that in the rodent hippocampus and neocortex CR-positive interneurons preferentially target other interneurons (Freund and Buzsaki 1996; Gonchar and Burkhalter 1999). Hence these cells are well suited to regulate and coordinate the activity of different GABAergic subclasses during a given network activity.

Labeling of neuronal cell populations with the in vivo marker enhanced green fluorescent protein (EGFP) revealed to be particularly useful for their systematic study in the acute slice preparation (Monyer and Markram 2004). To study CR-positive cells in the cortex we generated transgenic mice expressing EGFP under the control of the CR promoter. The analysis of EGFP/CR-positive cells led to the identification of 2 cell types with distinct biochemical, anatomical and physiological features, that we named bipolar CR cells (BCR cells) and multipolar CR cells (MCR cells).

The functional characterization comprised anatomical studies of biocytin-filled cells and patch-clamp recordings of individual labeled interneurons to establish their cellular properties as well as paired recordings to define the connectivity between EGFP/CR-positive interneurons and adjacent pyramidal cells or other GABAergic interneurons. We found that both types of CR-positive cells innervate mainly other interneurons but differ in their cellular and anatomical properties. Furthermore the electrophysiological studies indicated that the 2 cell types subserve different functions within a microcircuit.

Materials and Methods

Generation of CR-EGFP Transgenic Mice

A mouse 129SV strain BAC library (Research Genetics, Huntsville, AL) was screened for the CR gene by hybridization with an exon 1–derived 340-bp probe generated by PCR with the following primers 5′-ATGGCTGGCCCGCAGCAGCAGCCCC-3′ and 5′-GCCACCAGG-CAGCCGG-CATTCCCCG-3′. Hybridizing BACs were further analyzed for size following *Not*I digestion and pulse-field gel electrophoresis (PFGE) (CHEF-DRIII; Bio-Rad, Hercules, CA) and for the extent of 5′-flanking and 3′-flanking region of the CR gene by Southern blot of PFGE-resolved *Eag*I digested BAC DNA with suitable PCR-generated probes. Of the isolated BAC clones, clone 323F45 with an approx. size of 140 kb and containing >50 kb upstream and >40 kb downstream of the CR gene was chosen for transgene construction. A targeting vector was constructed to introduce a cassette of the EGFP coding sequence fused to the bovine growth hormone polyadenylation signal into the CR gene on BAC 323F45 such that the initiator methionine codon became the initiator codon for EGFP. The cassette was flanked by recombinogenic arms (RAs) spanning 540 bp 5′ and 291 bp 3′ of the initiator codon (Fig. 1), and generated by PCR with primers: 5′-GTCG-CTTCCAGTTGTCCACCTACG-3′, 5′-AGGGGGCTGCTGACGCGTGCCA-GCCATGGCGAGCC-3′, 5′-GCTCGCCATGGCTGGCACGCGTCA-GCAG-CCCCCTT-3′, and 5′-AGCCTCGAGGCAGCCGGCATTCCCCGAAA-3′,

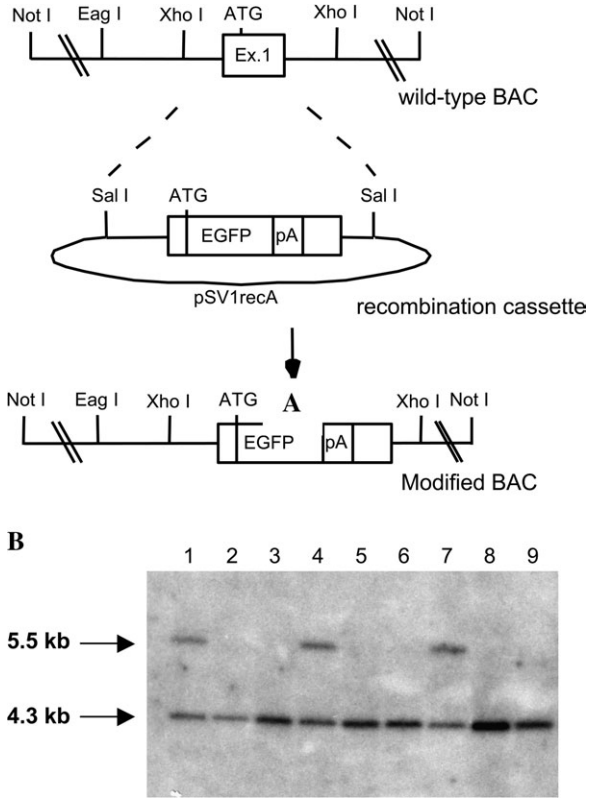

Figure 1. Generation of transgenic animals with EGFP expression in CR-positive neurons. (*A*) Schematic representation of the CR gene structure, the recombination cassette and the modified CR gene located on the BAC. Positions of *Xho*I, *Eag*I, and *Not*I restriction sites are indicated. (*B*) Southern blot analysis of tail DNA isolated from wild-type and transgenic mice, digested with *Xho*I to compare signal intensities of the wild-type (4.3 kb) and transgene (5.5 kb) band.

introducing a *Mlu*I site after the ATG and a *Xho*I site after the end of the 3′ RA. EGFP coding cassette and RAs were assembled by standard cloning techniques, and the correct sequence assembly was cloned into the *Sal*I site of the pSV1recA shuttle vector. For homologous recombination of the targeting cassette into the BAC, cointegrates were generated by transforming BAC-containing DH10B cells with pSV1.RecA-5′3′RA-EGFP DNA. Cointegration and resolution steps were as described (Meyer et al. 2002). The modified BAC DNA separated from bacterial genomic DNA by cesium chloride gradient ultracentrifugation was released from the vector by *Not*I digestion and isolated by sepharose column chromatography with column fractions analyzed by PFGE.

Purified, linearized BAC DNA (0.7 μg/mL) was microinjected into B6D2F2 mouse zygotes. Tail DNA of founders served to test integrity of the integrated BAC by PCR and Southern blot. Presence of the EGFP gene was assessed with the primers: 5′-ATGGTGAGCAAGGGC-GAGCT-3′ and 5′-GCCGAGAGTGATCCCGGCGGC-GGT-3′. The EGFP expression pattern was analyzed in transgenic mice, starting with the F2 generation. In 2 lines inheritance of the transgene followed Mendelian ratios, whereas in a third line no EGFP expression was detected.

Immunocytochemical Analysis of Expression in Transgenic Mice

P14 and adult (10–15 weeks old) transgenic animals were used to analyze EGFP expression and coexpression with CR. Animals were perfused with 4% paraformaldehyde (PFA)/phosphate-buffered saline (PBS; pH 7.4) and 50-μm-thick coronal sections were obtained from brain using a Leica VT1000S vibratome. The sections were washed in PBS 4 times for 10 min, permeabilized by incubation in PBST (PBS + 0.2% Triton X100) for 30 min and then incubated with mouse monoclonal CR (dilution 1:5000; Swant, Bellinzona, Switzerland), calbindin (1:2000; Swant, Bellinzona, Switzerland), or parvalbumin (1:5000; Sigma-Aldrich, St Louis, MO) and an EGFP rabbit antibody (1:10 000; Molecular Probes, Eugene, OR) in PBS for 12 h at 4°C. Incubated slices were washed 3 times with PBS for 10 min, incubated for 2.5 h with a 1:400 dilution of a Texas Red–conjugated anti-mouse IgG and Fluorescein-5-isothiocyanate (FITC)-conjugated anti-rabbit IgG (Jackson Immuno Research Laboratories, Inc, West Grove, PA) in PBS and subsequently washed twice in PBS for 10 min. Slices were protected from light during the procedure. Slices were mounted on slides, embedded in Mowiol (Polysciences, Warrington, UK), cover-slipped and analyzed using an upright fluorescent microscope (BX51 Olympus, Japan) equipped with a filter set for detection of FITC (excitation filter BP 450–490, dichroic mirror FT 510, and emission filter BP 515–565) and a filter set for detection of Texas Red (excitation filter BP 546/12, dichroic mirror FT 580 and emission filter LP 590).

Immunostainings using diaminobenzidine (DAB) as a chromogen were performed on P14 mice slices using the avidin–biotin–peroxidase technique with chemicals purchased from Vector Laboratories (Vectastain, ABCelite, Burlingame, CA).

Immunostaining of Biocytin-Filled Cells

After the electrophysiological recordings were performed with a pipette containing biocytin (Aldrich, Taufkirchen, Germany; 0.5–1 mg/mL), slices were fixed with 4% PFA for 30 min at room temperature. Slices were embedded in 4% agar (Fluka, Buchs, Switzerland), resectioned into 50-μm-thick sections on a vibratome (Leica VT1000S, Heidelberg, Germany) transferred into 50 mM Tris–HCl (pH 7.4), 1.5% NaCl (TBS, TRIS buffered saline). Sections were permeabilized in TBS, 0.4% Triton X-100 (Sigma, Steinheim, Germany) for 30 min followed by preincubation in TBS, 4% normal goat serum (NGS), 0.2% Triton X-100 for 30 min, and incubation in 2% NGS, 0.1% Triton X-100 at 4°C overnight with the antibody against CR (made in mouse, 1:5000). Sections were washed 3 times for 10 min with cold TBS and incubated for 2.5 h in the following mixture: FITC-conjugated avidin (3 μg/mL, Jackson Immuno Research, West Grove, PA) and Texas Red-conjugated anti-mouse IgG (1:400). After a brief rinse in bidistilled H_2O, sections were air dried and mounted in Mowiol. Immunostained sections were visualized under epifluorescent illumination with a BX51 microscope (Olympus, Japan).

Morphological Reconstructions

For morphological reconstruction cells were filled with biocytin (2%) added to the intracellular pipette solution. The slices were postfixed with 2% PFA overnight and cryoprotected with 30% sucrose. Subsequently they were permeabilized by freezing over liquid N_2, quenched in 1% H_2O_2 and incubated with avidin–biotin–horseradish peroxidase complex (Elite ABC, Vector Laboratories, Burlingame, CA). The immunoperoxidase reaction was developed using DAB (Sigma, St Louis, MO) intensified with nickel-sulfate (DAB–nickel) as chromogen. After development of the biocytin labeling with DAB–nickel–peroxidase, the slices were resliced into 60-μm-thick sections. The sections were osmificated and dehydrated in ascending alcohol series and in propylene-oxide followed by embedding into Durcupan (ACM, Fluka). Labeled cells (Forehand and Konopka 1989) were reconstructed using the Neurolucida tracing program (MicroBrightField, Colchester, VT). Polar analysis and measurements of cell somata were performed using the Neuroexplorer analysis program (MicroBrightField, Colchester, VT).

Electrophysiology

Sagittal neocortical slices of 250 μm were prepared from brains of P13–20 mice. Brain slices preparation and visualization of neurons were performed as previously described for rats (Markram et al. 1997). Thalamocortical slices (300–350 μm) thick were prepared as described in Agmon and Connors (1991). During recordings, slices were maintained at room temperature (22–24°C) except for the experiments studying oscillations (34–36°C). Slices were continuously superfused with an extracellular solution containing (in mM) 125 NaCl, 2.5 KCl, 25 glucose, 1.25 NaH_2PO_4, 2 $CaCl_2$ and 1 $MgCl_2$, bubbled with 95% O_2/5% CO_2. The pipette (intracellular) solution contained (in mM) 105 potassium gluconate, 30 KCl, 10 HEPES

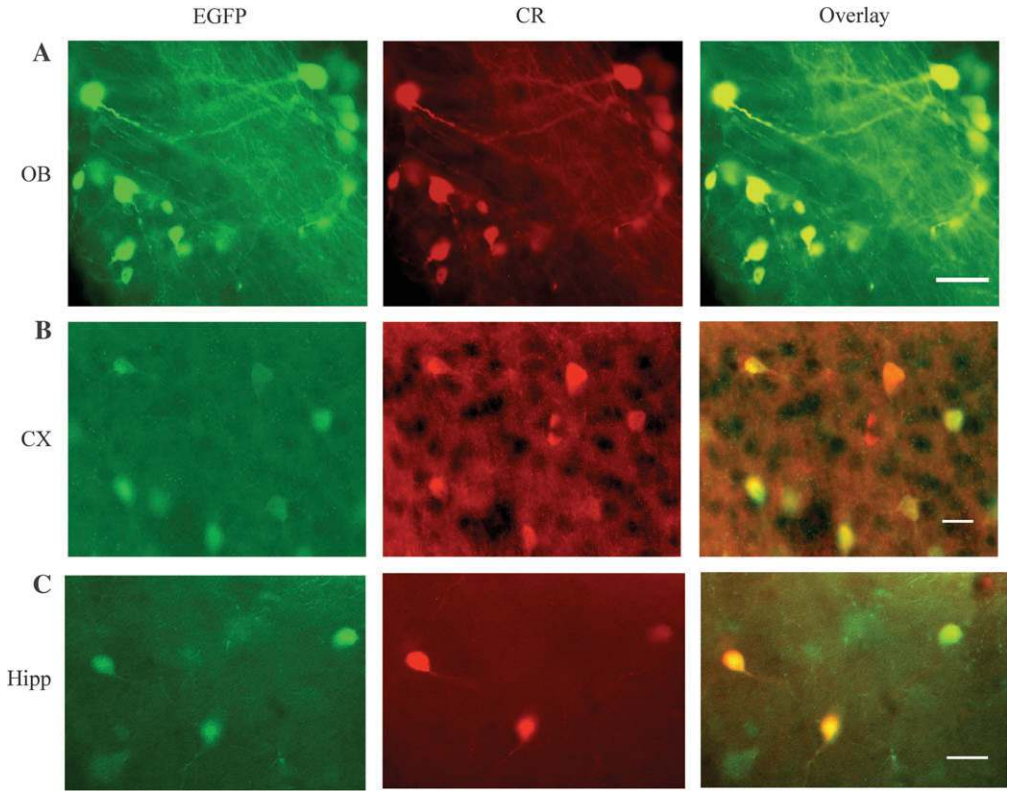

Figure 2. Colocalization of EGFP and CR expression in different brain regions of adult transgenic mice. EGFP (green, left panels) and CR (red, middle panels) immunocytochemistry show colocalization (right panels). (*A*) Olfactory bulb, glomerular layer. (*B*) Cortex layer 2/3. (*C*) Hippocampus CA1 area. Scale bars: (*A*) = 25 μm, (*B*, *C*) = 50 μm.

Table 1
Colocalization of EGFP and CR in the indicated brain areas of adult (10–15 weeks old) mice

Brain region	% CR- and EFGP-positive/ EGFP positive	% CR- and EFGP-positive/ CR positive
Prefrontal cortex (n = 46)	78.2	38.5
Motor and somatosensory cortex (n = 35)	79.3	42.6
Insular cortex (n = 38)	73.4	73.1
Stria medullaris (n = 91)	92.9	97.7
Medial horizontal nuclei horizontal limb diagonal band (n = 152)	91.6	75.2
Peryacqueductal gray (n = 92)	91.8	88.54
Cerebellar granular cells (n = 240)	93.7	88.46
Olfactory bulb glomerular layer (n = 253)	79.6	97.6
Olfactory bulb plexiform layer (n = 23)	13.1	1.2
Medial habenular (n = 98)	94.7	96.8
Central medial thalamic nuclei (n = 51)	93.7	85.7
Paracentral thalamic nuclei (n = 48)	16.7	100
Parasubthalamic nuclei (n = 33)	90	83.3
Reuniens nuclei (n = 67)	93	89
Dorsal geniculate lateral (n = 55)	96	94.6
Posterior nuclei (n = 66)	95.3	91.3
Hippocampus CA1 (n = 38)	89.9	23.4
Hippocampus DG (n = 52)	91.1	21.2

Note: n = number of cells.

(4-(2-hydroxyethyl)-1-piperazineethanesulfonic acid), 10 phosphocreatinine, 4 ATP-Mg, and 0.3 GTP (adjusted to pH 7.3 with KOH). In some experiments low chloride intracellular solution was used (in mM): 130 potassium gluconate, 4 KCl, 10 HEPES, 10 phosphocreatinine, 4 ATP-Mg, and 0.3 GTP (adjusted to pH 7.3 with KOH).

For electrophysiological recordings slices were placed in the recording chamber under an upright microscope (BX-51 WI; Olympus, Japan). Individual neurons were identified at 40× magnification using infrared-differential interference contrast (IR-DIC) microscopy and subsequent fluorescence microscopy.

Signals were recoded using IPC8 amplifiers (HEKA Electronics, Lambrecht, Germany), filtered at 3 kHz and digitized at 10 kHz, using an ITC-18 interface (Instrutech, Mineola, NY) and PULSE acquisition software (version 8.21; HEKA Electronics). Input resistances were derived from Ohm's law dividing the maximal averaged voltage deflection to 40 pA hyperpolarizing current pulses by the applied amplitude of the current pulse. Electrical coupling was tested as previously described (Venance et al. 2000). Voltage response was obtained by averaging 50 consecutive sweeps. The coupling coefficient was calculated as the ratio of the voltage response in cell 2 divided by the voltage response in cell 1 under steady state conditions. To measure junctional currents, electrically connected cells were held at −70 mV and negative or positive 100-ms voltage steps (50 mV) were injected in one of the cell and transmitted currents were recorded in the other, coupled cell.

To study synaptic connections, presynaptic cells were stimulated with a single pulse or with a 10 Hz train of 3 suprathreshold current pulses every 10 s. All recordings were carried out in current clamp mode. Postsynaptic cells were at resting membrane potentials unless otherwise stated.

To activate thalamic afferents, extracellular stimuli were delivered to the ventral basal (VB) thalamus via a platinum–iridium bipolar electrode (0.5 MΩ, 75 μm in diameter, purchased from Science Products, Hofheim, Germany). The cortex was initially mapped using extracellular recordings to find the barrel best aligned with the VB stimulation site (Beierlein et al. 2003). Simultaneous recordings were made in the aligned barrel in layer 4 cells (L4) cells and layer 2 pyramidal, MB or MCR neurons. The stimulus strength used to evoke responses in L4 cells was in the range of 20–350 μA and the pulse duration was 200 ms. Low chloride (4 mM) internal solution was used in this experiment to discriminate between excitatory postsynaptic potentials (EPSPs) and inhibitory postsynaptic potentials (IPSPs). To measure alpha-amino-3-

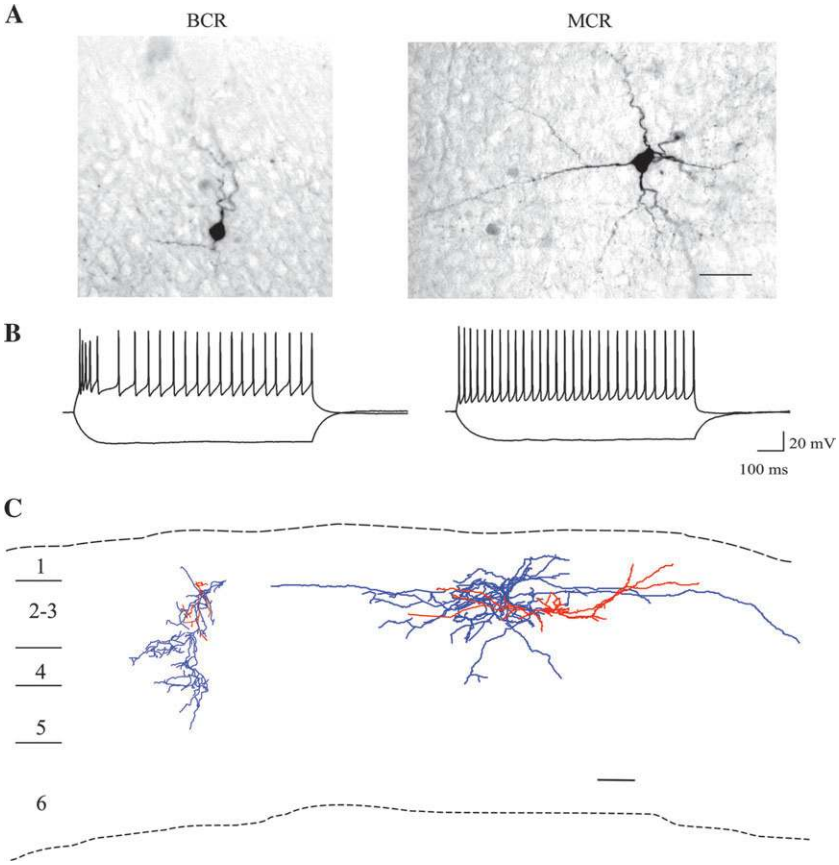

Figure 3. Morphology and firing pattern of BCR (left panels) and MCR (right panels) cells. (*A*) Biocytin-filled cells developed with DAB illustrating the bipolar and multipolar cell body shape of the 2 cell types. (*B*) BCR cells exhibit a bursting firing patter upon prolonged depolarized current injection, whereas MCR cells have an attenuating and "accommodating" firing pattern. (*C*) Reconstruction of 2 typical cells showing the preferential vertical and horizontal extension of BCR and MCR cell axons respectively. Scale bars: (*A*) = 30 μm, (*C*) = 100 μm.

hydroxy-5-methyl-4-isoxazolepropionic acid (AMPA) and N-methyl-D-aspartic acid (NMDA) receptor–mediated currents in thalamocortical slices, K^+ gluconate was substituted with equimolar Cs^+ gluconate in the intracellular solution. Gabazine (SR95531) was purchased from Biotrend, Zurich, Switzerland. Calculation of the statistical significance of differences was performed using Student's *t*-test unless otherwise specified. Data are presented as mean ± SD.

Results

Generation and Expression Analysis of the Transgene in CR-EGFP Mice

To generate mice expressing EGFP under the control of the CR gene promoter, we used a BAC containing the CR gene and approximately 50-kb upstream and 70-kb downstream sequences. The EGFP coding region was inserted into the CR start codon located on exon 1 (Fig. 1*A*). After pronuclear injection, 3 mouse-lines with full single-copy integration were obtained (Fig. 1*B*). EGFP expression studies revealed that the level and pattern was similar in 2 lines but no fluorescence was detected in the third.

In adult mice, strongest fluorescence was detected in areas known to express high CR levels such as the glomerular layer of the olfactory bulb (Fig. 2*A*). In periglomerular cells, EGFP fluorescence could be visualized even in dendrites. In other regions such as neocortex (Fig. 2*B*) or hippocampus (Fig. 2*C*), EGFP fluorescence was weaker and hence restricted to cell bodies.

To analyze the fidelity of transgene expression, we performed double immunostaining studies with EGFP- and CR-specific antibodies in adult mice (Table 1). There was variability of labeling (% of CR-positive cells expressing EGFP) with respect to brain areas. Thus, labeling was highest in brain regions with strongest CR immunoreactivity (e.g., cerebellum and olfactory bulb). Colocalization studies (% of EGFP-positive cells expressing CR) revealed a good overall correspondence except for a few regions (e.g., plexiform layer of the olfactory bulb and the paracentral thalamic nuclei). Occasional EGFP expression in some astrocytes was also detected (data not shown) but this "misexpression" was not problematic because cell types were verified electrophysiologically in this study.

As for most patch-clamp recordings (including our own, see below) employing slices from juvenile animals are used, we analyzed the colocalization also in P14 mice. In neocortex the percentage of EGFP-positive cells expressing CR was comparable to that in adult animals (76%, 57/75 obtained from 3 transgenic mice). In hippocampus most cells correctly expressed EGFP (85.9%, 67/78) but there was some misexpression in a few CA1 pyramidal cells. In other brain areas such as cerebellum (95.9%, 165/172), olfactory bulb (92.5%, 137/148), and thalamus (57.3%, 82/143), the extent of colocalization in P14 mice was similar to that observed in the adult. However, the EGFP signal was stronger in acute slices from juvenile animals. In fact after P22 the EGFP signal was difficult

to detect in acute cortical and hippocampal slices, but continued to be strong in other brain region such as cerebellum, olfactory bulb, and thalamus. Nevertheless, EGFP could be detected in cortex and hippocampus by immunohistochemistry as mentioned above.

CR-positive Cells in Cortical Layer 2/3 Comprise Two Distinct Subtypes

The functional studies in acute neocortical slices (P14–20) focused on layer 2/3 EGFP/CR-positive cells because the results allowed a comparison with those obtained for other interneurons in previous studies (Reyes et al. 1998; Rozov et al. 2001; Blatow et al. 2003). Based on the cell body appearance when viewed with IR-DIC microscopy, EGFP-positive cells could be divided into BCR and MCR cells (Fig. 3*A*). BCR cells had an elongated soma with one or 2 dendrites that were oriented mainly vertically (Fig. 3*A*, left panel). MCR cells had round cell bodies with multiple primary dendrites (Fig. 3*A*, right panel). BCR and MCR cells could be also distinguished based on their action potential (AP) firing pattern. In BCR cells, prolonged depolarizing current injection evoked an initial burst of 2 or 3 APs (burst frequency of 82 ± 22 Hz) followed by a subsequent train of regularly low frequency spiking APs (22 ± 3 Hz; Fig. 3*B*, left panel). MCR cells exhibited a different firing pattern that was characterized by a pronounced attenuation of AP amplitude and accommodation of the firing frequency (Fig. 3*B*, right panel). The basic electrophysiological properties of BCR and MCR cells are summarized in Table 2 and are compared with those obtained for the parvalbumin-positive cells of the MB (multipolar bursting) and FS (fast spiking) type. The identification in acute slices of latter 2 interneuron types, that were EGFP-negative was based on criteria as previously described (Blatow et al. 2003; Reyes et al. 1998; Rozov et al. 2001). Briefly, FS cells were recognized by their multipolar appearance in the IR-DIC video image and by their ability to fire APs at high frequency upon prolonged depolarizing current injection (Supplementary Fig. 1 and Table 2). MB cells could be recognized by their location close to the border between layers 1 and 2 and their morphological appearance in the IR-DIC image (Supplementary Fig. 1). These neurons have large round or oval cell bodies and one or several visible thick dendrites. Their AP firing pattern upon prolonged depolarizing current injection is characterized by an initial burst of few APs followed by an after-hyperpolarizing gap and a subsequent train of regular spiking, low frequency APs. A striking difference was the input resistance that was significantly higher in BCR and MCR cells than that of the other 2 GABAergic interneuron subtypes. Input resistance values for MB, BCR and MCR cells did not change significantly at physiological temperature.

To establish the correct EGFP expression in BCR and MCR cells at the cellular level, the presence of CR was verified by immunolabeling in identified cells. Biocytin-filled BCR (7 out of 7) and MCR cells (9 out of 9) were indeed CR-positive (Fig. 4*A*,*B*) thus corroborating the correct transgene expression in these cells. It was reported in previous studies that BCR-positive interneurons with a firing pattern resembling the one described here for BCR cells also expressed VIP (Cauli et al. 1997; Rozov et al. 2001). Interestingly, BCR and MCR cells differed with respect to VIP immunoreactivity: 6 out of 7 biocytin-filled BCR cells were also VIP-positive (Fig. 4*C*), whereas MCR cells were VIP-negative (0 out of 7 cells; Fig. 4*D*).

Table 2
Electrical parameters of MCR and BCR cells compared with MB and FS cells

Cell type	Input resistance (MOhm)	Vm (mV)	Threshold potential (mV)	AP half width (ms)	AP amplitude (mV)	AP attenuation (% of amplitude)	Interspike interval (ms)	AP accommodation (% of IS interval)	Main firing frequency (Hz)	Burst frequency (Hz)	AHP duration (ms)	Membrane time constant (ms)
MCR, $n = 13$	558 ± 170	−64 ± 3	−41 ± 3	1.4 ± 0.2	74 ± 5**	82 ± 6	23 ± 6	218 ± 6	31 ± 8	—	—	45.8 ± 14.3
BCR, $n = 10$	675 ± 163	−66 ± 2	−41 ± 3	1.5 ± 0.2	67 ± 2**	—	—	—	22 ± 3	82 ± 22	66 ± 17	43.2 ± 8.9
MB, $n = 11$	111 ± 39	−60 ± 3**	−43 ± 3	0.9 ± 0.3	81 ± 9	—	—	—	13 ± 2**	71 ± 20	166 ± 37	22.7 ± 7.2
FS, $n = 11$	82 ± 31	−73 ± 3**	−37 ± 3	0.7 ± 0.1	77 ± 6	—	—	—	38 ± 9**	—	—	10.4 ± 2.4

Note: All measurements were performed at room temperature. Input resistances were derived from Ohm's law dividing the maximal averaged voltage deflection to 40 pA hyperpolarizing current pulses by the applied amplitude of the current pulse. Firing properties were analyzed upon 500 pA current injection for 1 s for all cell types. AP half widths and amplitude were measured on the first AP in the train upon depolarizing current injection at threshold level. AP attenuation and accommodation were measured as a change of initial amplitude and interspike interval at the beginning and at the end of the AP train. AHP duration was measured as the time from the end of the initial burst to the regular spiking part of the firing pattern. Vm = resting potential; IS = interspike; AHP = after-hyperpolarization. Attenuation and accommodation were expressed as percentage of initial amplitude and interspike interval to the vales measured at the end of AP train.

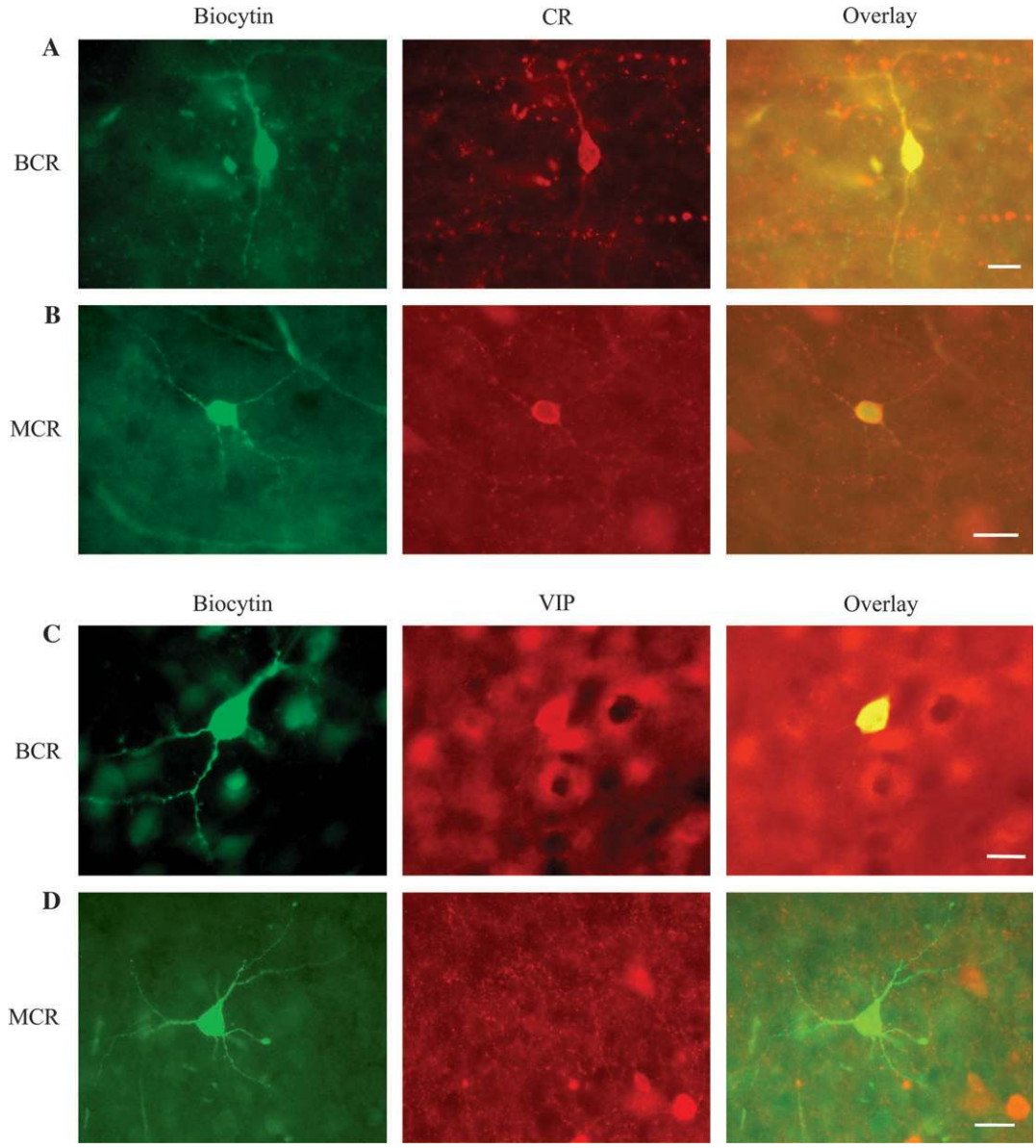

Figure 4. Bipolar and multipolar biocytin-filled EGFP-positive cells are CR-positive and differentially express VIP. (*A*, *B*) Typical bipolar and multipolar EGFP-positive cell in cortical layer 2/3 expressing CR. (*C*, *D*) BCR but not MCR cells are VIP-positive. Slices were obtained from P14 to P18 mice. Scale bars: 25 μm.

No or little colocalization was observed between EGFP and parvalbumin (0 out of 181) or EGFP and calbindin (5 out of 157) in cortical layer 2/3 of P15 mice.

For a detailed morphological analysis, biocytin-filled BCR ($n = 9$) and MCR ($n = 13$) cells were reconstructed (Fig. 3*C* and Supplementary Fig. 2). Both BCR and MCR cells had smaller cell bodies (perimeter: 32.5 ± 5.8 and 36.3 ± 7.2 μm, respectively) than layer 2/3 pyramidal neurons (70.4 ± 12.3μm) or MB cells (64.2 ± 9.3 μm). BCR cells had one or 2 vertically oriented dendrites (1.8 ± 0.4) extending most often from layer 1 to layer 4, whereas MCR cells had multiple primary dendrites (4.8 ± 1.2) with a preferential horizontal extension within the cortical layers 1–3. Figure 5*A* shows the bimodal distribution of the number of primary dendrites in these EGFP/CR cells, corresponding to the 2 cell types (chi square test: $P < 0.001$). BCR and MCR cells differed also with respect to their axonal arborization. The former extended mainly vertically reaching layer 5, whereas the preferred horizontal extensions of the latter were mainly found within layers 2/3 of the neocortex. Histograms in Figure 5*B* represent the polar extension of axon and dendrites of the 2 cells types in cortical layer 2/3.

Synaptic Connectivity and Dynamic Properties of Synapses of CR-positive Interneurons

The functional role of a certain cell type within a microcircuit is determined by the wiring pattern and the differential properties of the synapses involved. In rat hippocampus CR-positive interneurons do not target excitatory cells (Freund and Buzsaki 1996; Gulyas et al. 1996). Hence we investigated whether this characteristic also holds true for CR-positive cells in neocortical layers 2/3. We studied the presence of chemical synapses between the 2 CR-positive cell types and pyramidal cells. Furthermore, we analyzed their connectivity with 2 other

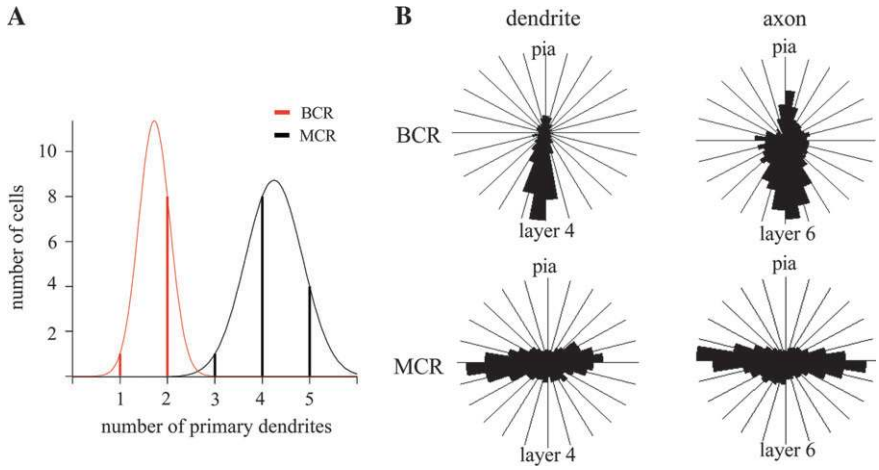

Figure 5. Anatomical differences between BCR and MCR cells. (*A*) Bimodal distribution of primary dendrite numbers of reconstructed BCR and MCR cells. Nine BCR and 13 MCR neurons were selected based on their firing patterns and the number of their primary dendrites was plotted. Gaussian distribution curves fit for both cell types (chi square $<$ 0.001). (*B*) Polar histogram of dendrites and axons of 9 BCR and 13 MCR reconstructed cells showing the different dendrites and axon extension for the 2 cell types.

types of GABAergic interneurons and with themselves. Finally we examined the dynamic properties at all these synapses.

To investigate the connectivity of CR-positive cells we performed simultaneous paired whole-cell recordings. The maximal distance between pre- and postsynaptic cells was 150 μm. BCR and MCR cells received excitatory synaptic input from layer 2/3 pyramidal cells (success rate ~18% for both connections). The 2 types of connections had comparable connectivity rate, but they expressed different dynamic properties of synapses. To determine the dynamic properties of synapses, a 10 Hz train of APs was elicited in presynaptic cells and the ratio between the second and the first postsynaptic potential (PSP) was calculated. Excitatory input from layer 2/3 pyramidal cells to BCR cells showed paired pulse depression, whereas the excitatory input to MCR cells exhibited prominent paired pulse facilitation. In the opposite direction, from BCR or MCR to layer 2/3 pyramidal cells, the connectivity was low (success rate 11% for BCR to pyramidal cells and 14% for MCR to pyramidal cells connections, Fig. 6*A* and *B*; Table 3). Thus, BCR and MCR cells differ in this respect from MB and FS neurons that target pyramidal cells more frequently (about 50% of tested pair; Gupta et al. 2000; Wang et al. 2002; Blatow et al. 2003; Holmgren et al. 2003). Differential dynamic properties of synapses for the 2 cell types was also found in this direction: paired pulse facilitation was found at BCR to pyramidal cell synapses and paired pulse depression at MCR to pyramidal cell synapses.

Next we tested the connectivity of BCR and MCR with MB and FS cells (Fig. 6*C,D*). BCR cells innervated MB cells in a unidirectional way with a connectivity rate of 27%. This connection exhibited pronounced paired pulse facilitation. We could not find a connection in the opposite direction. BCR neurons were reciprocally connected with FS cells with success rates of 30% for both directions.

MCR cells were reciprocally connected to MB interneurons with a higher connectivity rate for MCR to MB cells (success rate = 50%) than for MB to MCR cells (success rate =18%;). MCR and FS cells were reciprocally connected (success rate = 18%). Inputs from MCR to FS cells showed paired pulse facilitation. The connectivity in the opposite direction, FS to MCR cells, was similar (success rate = 20%), but the connections were characterized by prominent depression.

Table 3
Connectivity and dynamic properties of synapses of CR-positive cells

Connections	Attempts	Success	Success rate (%)	PPR	SD
Pyr–BCR	60	11	18.3	0.6*	0.1
FS–BCR	37	11	29.7	0.6	0.1
MB–BCR	43	0	0	0	0
Pyr–MCR	63	11	17.4	1.6*	0.7
FS–MCR	55	11	20	0.7	0.2
MB–MCR	22	5	22.7	0.8	0.1
BCR–Pyr	60	7	11.6	1.4***	0.2
BCR–FS	37	11	29.7	1.1	0.2
BCR–MB	43	13	30.2	1.8	0.3
BCR–BCR	22	7	31.8	1.42#	0.2
BCR–MCR	17	13	76.4	1.33**	0.3
MCR–Pyr	63	9	14.2	0.7***	0.3
MCR–FS	55	10	18.1	1.4	0.4
MCR–MB	22	11	50	1.1	0.4
MCR–BCR	17	7	41.1	0.98#	0.2
MCR–MCR	71	7	9.8	0.74**	0.3

Note: PPR= paired pulse ratio calculated as second/first mean amplitude. Symbols (*, **, ***, and #) denote types of cell pairs that were compared and have statistically different PPRs. $P < 0.01$.

Finally, we studied the connectivity between CR/EGFP-positive cells (Fig. 6*C,D*). BCR cells often targeted MCR cells (success rate = 80%;), and the chance of finding MCR to BCR cell connections was 40%. Connectivity between BCR cells was higher (success rate = 30%) than between MCR cells (success rate only = 10%). The connectivity and the dynamic properties of the synapses of all the cells analyzed are summarized in Table 3.

Thus, BCR and MCR cells exhibited differential connectivity with neighboring identified cells. Both cell types rarely innervated nearby located pyramidal cells but preferentially targeted other interneurons. The success rate of BCR cells targeting MB, FS or other BCR cells was comparable whereas MCR cells targeted preferentially MB and BCR cells. Of note is the very high connectivity rate from BCR to MCR cells and the absence of connections from MB to BCR cells. Another distinct feature of BCR cells is that they always established facilitating connections with the target cells.

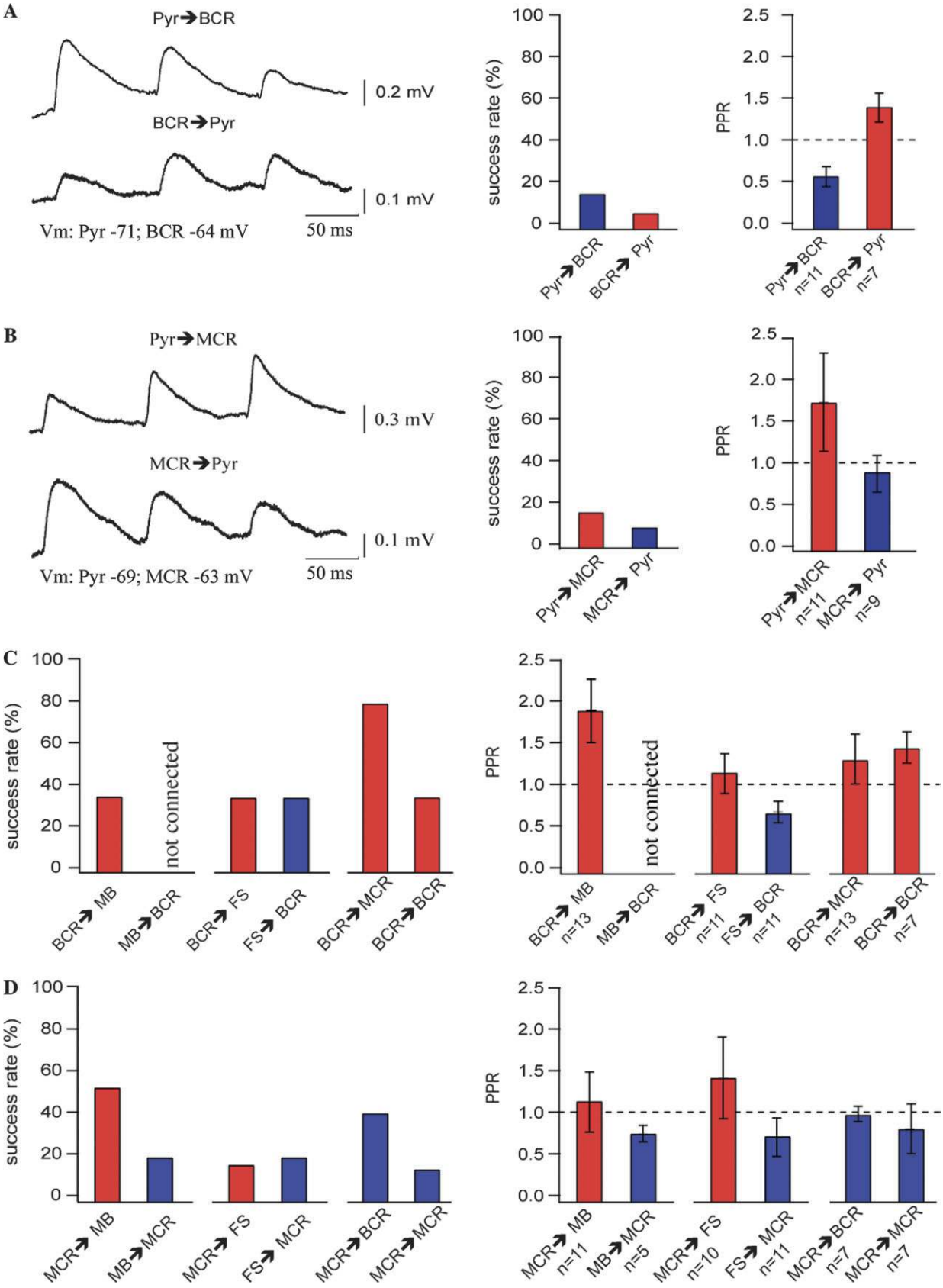

Figure 6. Connectivity and dynamic properties of synapses of CR-positive cells. Paired whole-cell recordings from CR-positive and adjacent pyramidal, FS and MB cells. (*A*, *B*) Connectivity between BCR (*A*) or MCR (*B*) and pyramidal cells. Left panel: average traces of postsynaptic responses to a 10 Hz train of 3 APs. Each trace represents the average of 100 subsequent sweeps recorded at room temperature. 30 mM chloride intracellular solution was used to improve signal/noise ratio increasing the chances to detect weak connections. Under these conditions the reverse potential is around −30/−40 mV and IPSPs are depolarizing. Histograms summarize the success rate for the respective type of

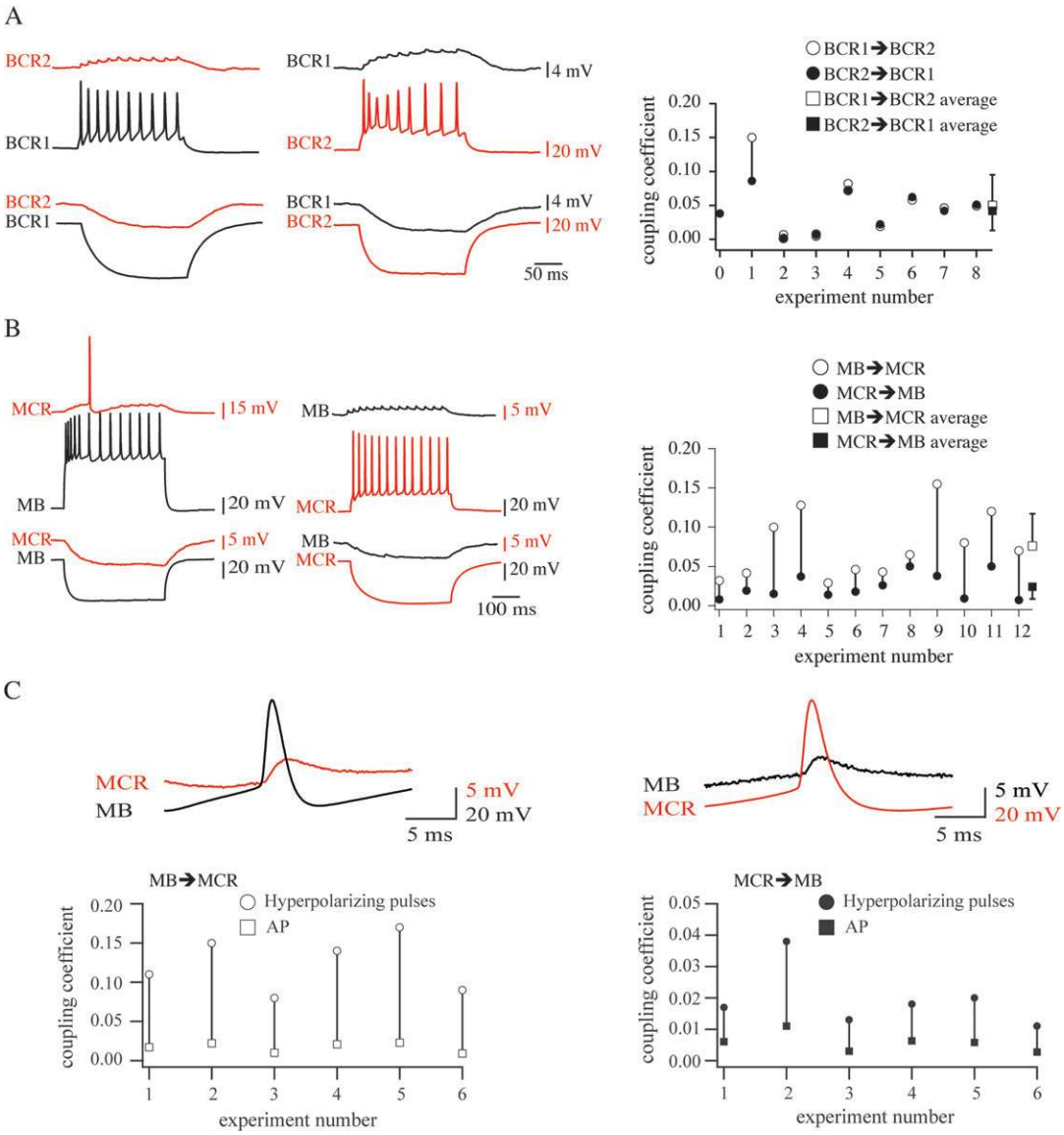

Figure 7. Electrical synapses of CR-positive cells. (*A*) BCR cells are reciprocally coupled via gap junctions. Left panel: DC coupling between 2 BCR cells. Depolarizing or hyperpolarizing current injection into cell 1 evokes voltage responses in cell 2. APs in cell 1 were reflected as spikelets in cell 2. Gap junction coupling is always reciprocal. (*B*) MCR and MB cells are reciprocally and asymmetrically coupled via gap junctions. Left panel: DC coupling between MCR and MB cells. Gap junction transmission efficiency was always higher in the direction from MB to MCR cells as indicated by higher coupling coefficient values. APs in MB cells were reflected in MCR cells either as spikelets or as APs. Right panels: histograms represent coupling coefficient in the individual pairs. Note the difference in the coupling coefficient depending on whether current was injected into the MB or MCR cell. (*C*) Electrical synapses between MB and MCR cells behave as low pass filters. The efficiency of transmission for fast events like APs is lower than that for long-lasting hyperpolarizing pulses. Left traces show an AP evoked in an MB cell and the corresponding spikelet recorded in an MCR cell; right traces show the reciprocal experiment. Coupling coefficient for AP transmission was calculated as a ratio of AP and spikelet amplitude. Histograms compare differences in coupling coefficients between slow and fast events.

Electrical Coupling of CR-positive Cells

Several studies have shown that GABAergic interneurons are coupled via gap junctions. Most often the coupling is bidirectional and occurs between GABAergic interneurons of the same type (Hestrin and Galarreta 2005). Hence, we studied whether, in addition to uni- or bidirectional chemical transmission, BCR and MCR cells were electrically coupled in a cell type-specific manner.

Indeed, when 2 BCR cells were found close to each other (within 100 μm) they were often coupled via gap junctions (success rate 60%, 9 out of 15, Fig. 7*A*). Electrical coupling between BCR cells was symmetric and the strength of DC coupling measured as coupling coefficient was 0.05 ± 0.06. In contrast, gap junction coupling was never found between MCR cell pairs (n = 70). However, MCR cells were electrically coupled with MB cells (success rate 63%, 12 out of 19, Fig. 7*B*).

connection (middle panels) and show the averaged paired pulse ratio (PPR) of postsynaptic potentials (right panels). Vm = membrane potentials. (*C*, *D*) Connectivity between BCR (*C*) or MCR cells (*D*) and other interneurons. Histograms summarize the success rate for the respective type of connection (left panels) and show the averaged PPRs of IPSP (right panels). Pyr, pyramidal cells. See Table 3 for the statistical analysis of the connectivity between these cells.

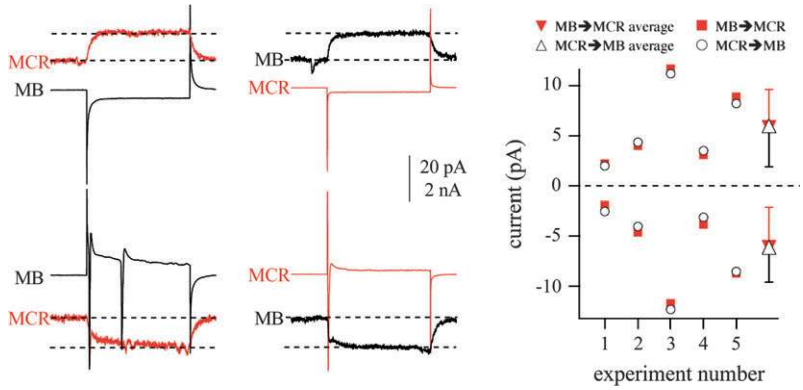

Figure 8. Gap junctional currents between MB and MCR cells are identical in amplitude. Upper traces show representative junctional currents recorded from MCR and MB cells upon hyperpolarizing voltage injections to either MB (left) of MCR cells (right). Lower traces show similar experiments for depolarizing voltage steps. Note that the current amplitude was similar in both cell types. Scatter plot summarizes data from individual pairs. Circles represent junctional currents recorded from MB cells and squares from MCR cells.

Interestingly, DC coupling between MCR and MB cell pairs was asymmetric: a coupling coefficient of 0.02 ± 0.06 was calculated when current was injected into MCR cells and responses were recorded in coupled MB cells whilst the coupling coefficient in the opposite direction was 0.07 ± 0.03. In fact, in 4 out of 12 cases, AP firing in the MB cell could trigger APs in the coupled MCR cell. Gap junctions are known to behave as low pass filters (Galarreta and Hestrin 1998; Bennett and Zukin 2004; Price et al. 2005). To evaluate filter properties of the asymmetrical electrical synapses between MB and MCR cells, we compared coupling coefficients for transmission of short-lasting and fast-rising APs with those for transmission of long-lasting hyperpolarizing currents. Figure 7*C* shows example traces of APs and corresponding spikelets for MB and MCR cells. In the panels underneath, coupling coefficients of short-lasting and long-lasting alterations of membrane potentials are compared. When currents were injected into MB cells and responses recorded in MCR cells, coupling coefficients were 0.017 ± 0.005 and 0.12 ± 0.035 for AP transmission and long pulses respectively ($n = 6$). For the opposite direction, coupling coefficient for AP transmission was 0.006 ± 0.003 and for long hyperpolarizing pulses 0.02 ± 0.01 ($n = 6$). Filtering properties were more pronounced in the MB to MCR cell direction. The ratio between coupling coefficients of AP- and long-lasting transmission was significantly smaller in the MB to MCR cell direction (0.14 ± 0.01) than in the opposite direction (0.29 ± 0.05, $P < 0.01$). This difference most likely results from the longer membrane constant in MCR (45.8 ± 14.31) than in MB cells (22.7 ± 7.2, see Table 2).

Most likely the asymmetry of electrical synapses between MB and MCR cells as well as the higher excitability of MCR neurons are due to the higher input resistance of MCR cells than that of MB cells (see Table 1). To directly test this we measured in voltage clamp mode junctional currents between MB-MCR cell pairs (Fig. 8). In these experiments both cells were held at –70 mV. When 50 mV hyperpolarizing voltage steps (100 ms) were injected in one cell resulting in an inward current, an outward current could be measured in the coupled cell. Amplitudes of junctional currents were identical in both cells (5.98 ± 4.1 and 5.85 ± 3.77 pA for currents measured in MB and MCR cells respectively). Similar results were obtained when cells were injected with depolarizing voltage steps (–6.1 ± 4.0 and –6.1 ± 3.5 pA for MB and MCR cells). Absolute values of evoked junctional current did not depend on the polarity of current injection. Data from 5-cell pairs is summarized in the plot on the right panel (Fig. 8*C*). These data confirm that the apparent asymmetry of electrical synapses between MB and MCR cells is not due to rectification of gap junction channels, but rather to differences in cellular properties such as input resistance.

Integration of MB and MCR Cells into Cortical Networks

Electrical synapses between cells have been considered as an important determinant of synchronous activity at a network level. The fact that MB and MCR cells are specifically coupled via gap junctions indicates that they might functionally belong to the same network.

In a previous study (Blatow et al. 2003) we characterized the role of MB cell inhibitory network in an "in vitro" model of membrane oscillations (5.2 ± 1.17 Hz) induced by carbachol bath application. We had characterized this model and showed that the rhythmic activity of MB cells led to synchronized IPSPs in layer 2/3 pyramidal cells thereby phase-locking their firing activity. Rhythmic activity required activation of muscarinic receptors, GABAergic transmission and gap junction coupling. Here we tested whether MCR cells are also involved in this functional network. The experimental procedure was identical to the one described in a previous paper (Blatow et al. 2003). Activity from 18 pairs of MB and MCR cells was recorded upon bath application of 40 μM carbachol. Carbachol-induced synchronized sub- or suprathreshold rhythmic membrane potential oscillation with a frequency range of 4.5–11.8 Hz when MB and MCR cells were electrically coupled. Although membrane oscillations in both cell types were in the same frequency range, no synchronization was observed when the coupling coefficient was lower than 0.01 ($n = 6$, Fig. 9*A*) or when cells were not coupled ($n = 4$). However, when the coupling coefficient was higher (Fig. 9*B*), synchrony increased proportionally ($R = 0.91$; $P < 0.01$; $n = 8$; Fig. 9*C*). We had already shown that upon carbachol application, membrane oscillations in pairs of MB cells were always synchronized (43 out of 43; Blatow et al. 2003), not depending on the strength of DC coupling. Because synchrony between MB and MCR cells was crucially dependent on the strength of electrical coupling, we can assume that these 2 cell types belong functionally to the same cortical network where MB cells can drive MCR cells.

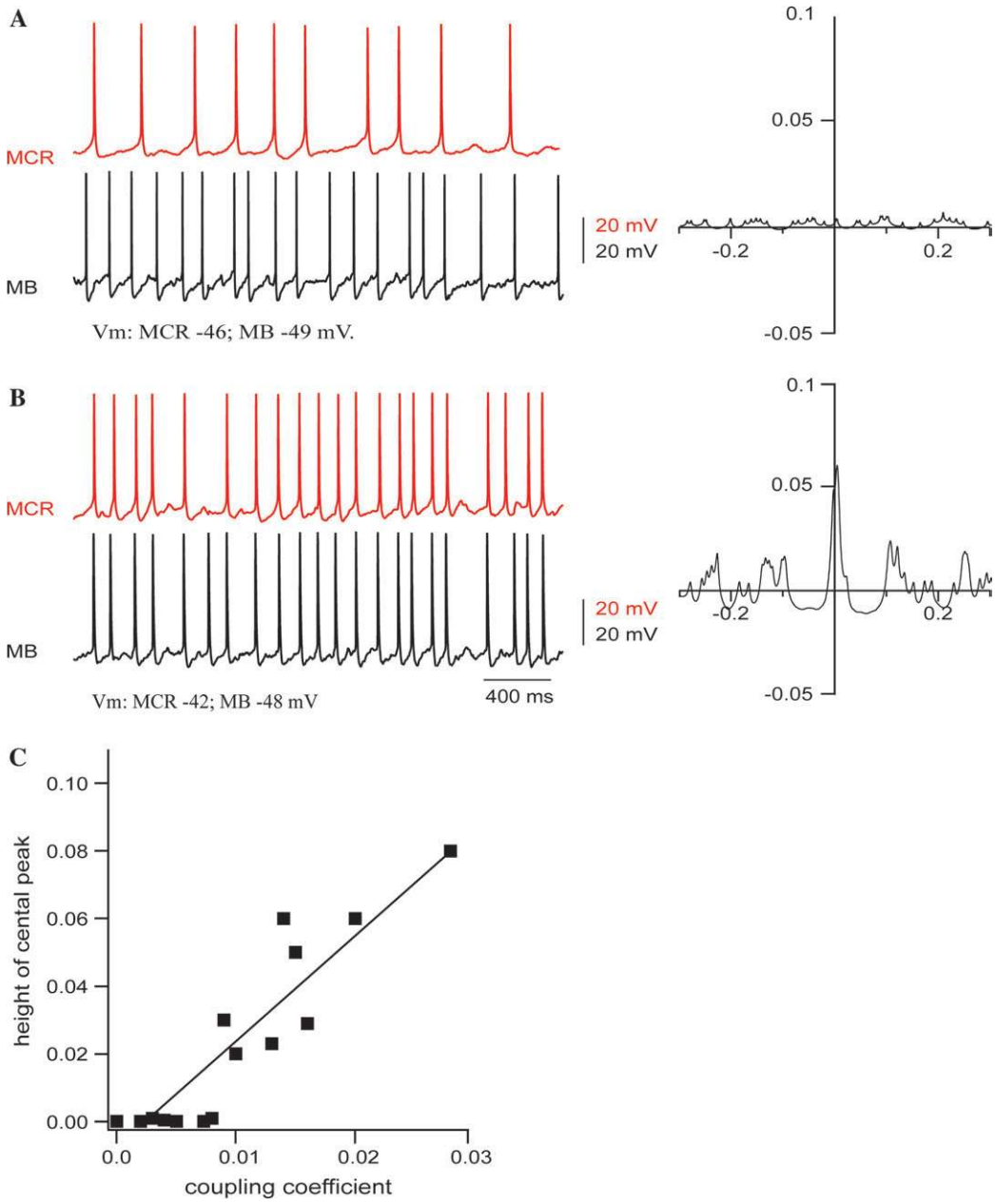

Figure 9. Carbachol-induced synchronous rhythmic activity in MCR (red) and MB cells (black) requires strong gap junction coupling. (*A*) 40 μM carbachol-induced activity was not synchronous (left panel) as evidenced by the cross-correlogram (right panel) when the strength of coupling was weak (coupling coefficient 0.005). (*B*) 40 μM carbachol-induced activity was synchronous (left panel) as evidenced by the cross-correlogram (right panel) when the coupling was strong (coupling coefficient 0.015). (*C*) Plot shows the dependence of synchrony (height of central peak of the cross-correlograms) on the coupling coefficient between MB and MCR cells. No synchrony was detected when the coupling coefficient was < 0.008 ($n = 6$) or when cells were not coupled ($n = 4$). When the coupling coefficient was > 0.008, synchrony increased proportionally ($R = 0.91$; $P < 0.01$; $n = 8$). Coupling coefficient was calculated for the MB to MCR cell direction. Vm = membrane potentials.

Next, we sought whether MB and MCR cells are differentially excited by neuronal populations located in different cortical layers. Given that the columnar organization and the excitation flow within the barrel cortex has been extensively characterized (Douglas and Martin 2004; Lubke and Feldmeyer 2007), we tested how excitation spreads from thalamus to MB and MCR cells, respectively. To this end we used thalamocortical slices, a frequently used preparation to study excitation spreading within barrel cortex (Llinas et al. 2002; Cruikshank et al. 2007; Tan et al. 2008). We analyzed the synaptic latencies of EPSPs evoked in these interneurons upon extracellular stimulation in the thalamus. A bipolar stimulating electrode was placed in VB thalamus and recordings were carried out in cells located in the best-aligned barrel. As reference we used the synaptic latencies in layer 4 adaptive/regular firing (L4) cells known to receive monosynaptic inputs (Koralek et al. 1988; Chmielowska et al. 1989; Lu and Lin 1993). First using minimal stimulation, we determined stimulation threshold for L4 cells that was in the range of 20–350 μA. Four L4 cells were biocytin filled and reconstructed; all 4 cells showed the typical morphology of spiny stellate cells (Supplementary Fig. 3). Subsequently, MB, MCR, and neighboring layer 2/3 pyramidal

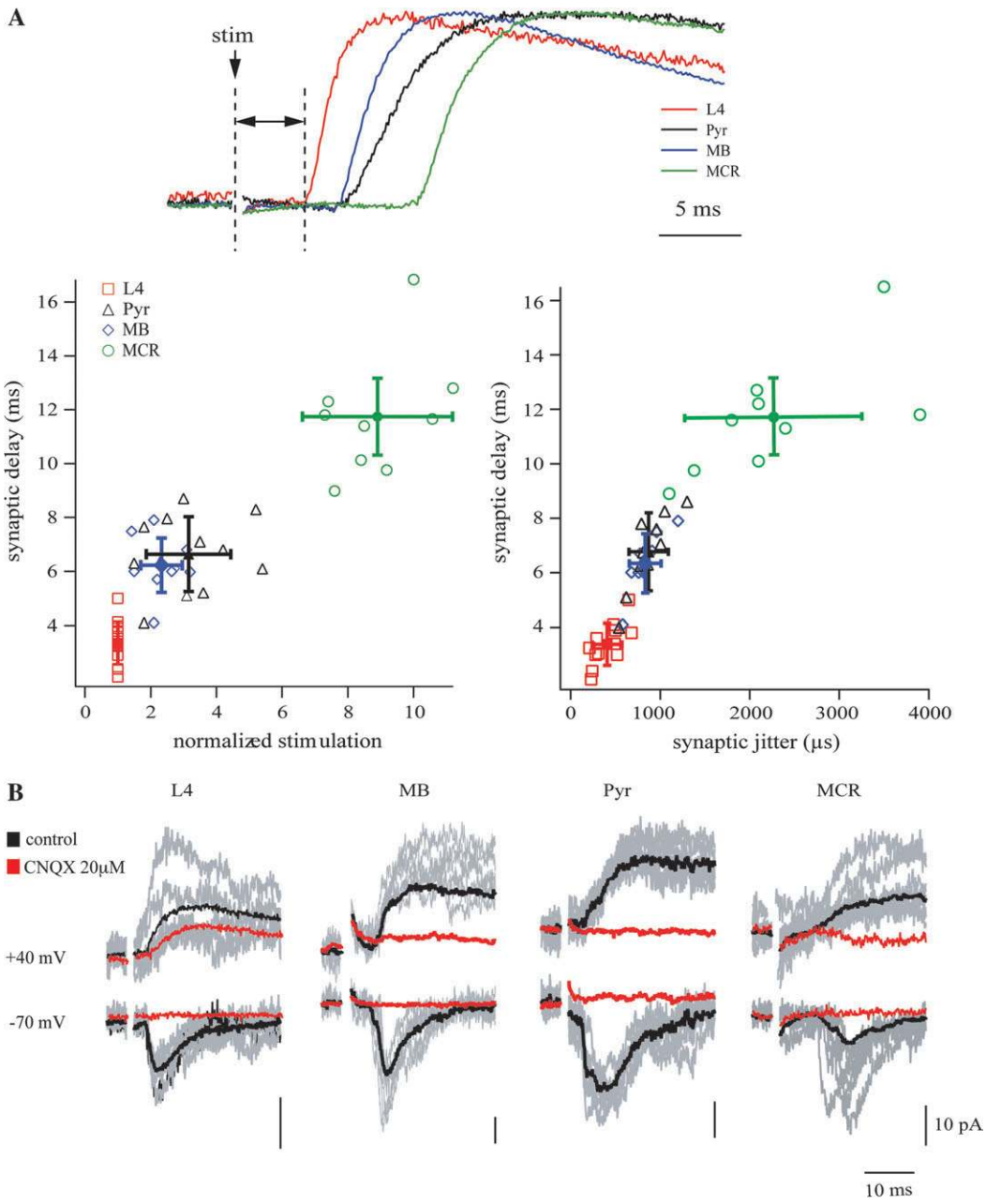

Figure 10. Onset latencies and synaptic jitter of evoked postsynaptic potentials differ between MB and MCR cells. (*A*) Representative average traces of PSP recorded from layer 4 adapting/regular spiking (L4), layer 2 pyramidal (Pyr), MB and MCR cells upon thalamic stimulation. Synaptic latency was measured from the beginning of the stimulus artifact to the onset of PSP. Traces were scaled to the same amplitude. Left panel represents synaptic latencies for EPSPs elicited in L4, layer 2/3 pyramidal, MB and MCR cells are plotted against threshold stimulus intensity. Stimulus strengths were normalized against the minimal stimulus required to elicit an EPSP reliably in a L4 cell in the same experiment. Right panel represents the dependence of synaptic jitter on absolute latency. Jitter was expressed as the standard deviation of absolute latency and, as expected, jitter values were higher in cells with longer latencies. Open symbols represent averaged data for individual cells. Closed symbols show averaged data for each group. (*B*) Synaptic responses recorded upon thalamic stimulation in the 4 cell types at +40 mV (upper traces) and −70 mV (lower traces) before (black traces) and after (red traces) blocking AMPA receptor–mediated currents with 20 μM CNQX. Gray traces represent an overlay of 5 consecutive responses (failures are excluded) under control condition. In the presence of CNQX, NMDA receptor–mediated responses can be detected only in L4 cells, confirming the monosynaptic thalamic input. Absence of NMDA receptor–mediated responses in the other cell types confirms the polysynaptic nature of evoked EPSCs.

cells were sequentially patched in upper layer 2 of the same barrel. Stimulus intensity was increased to a value minimal and sufficient to evoke responses in interneurons or pyramidal cells and 100 sweeps were collected. For analysis, the intensity of the threshold stimulus in layer 2 cells was normalized to that obtained for L4 cells and plotted as a function of synaptic latency (Fig. 10*A*). As expected, the direct monosynaptic thalamic input to L4 cells was reflected in the short synaptic latency (3.35 ± 0.79 ms). The synaptic latencies for MB and layer 2/3 pyramidal cells were twice as long (6.23 ± 1.1 and 6.64 ± 1.39 ms) and the required stimulus intensities were 2–3 times higher (2.33 ± 0.63 and 3.16 ± 1.29, respectively; Fig. 10*A*) than for L4 cells, indicating that these cells receive disynaptic excitatory input from thalamus, and implying a direct excitation from layer 4. Values for MB cells (both synaptic latencies and normalized stimulus intensities) were slightly

lower than those of layer 2/3 pyramidal cells, excluding the possibility that the recorded responses could be due to activation of layer 2 excitatory microcircuits. To trigger responses in MCR cells the stimulus intensity was on average 9 fold higher than the one in L4 cells (8.90 ± 1.42), and the synaptic latency was significantly longer (11.74 ± 2.2 ms) than the ones in MB and layer 2/3 pyramidal cells (Fig. 10*A*). Both the length and the variability in the onset latencies for MCR EPSPs suggest a tri- rather than a disynaptic pathway from thalamus to MCR cells. Next, we determined EPSP jitter as it has been shown that this analysis provides better discrimination between mono- and polysynaptic pathways (Doyle and Andresen 2001). The right plot in Figure 10*A* illustrates the relationship between synaptic jitter and absolute latencies. The lowest jitter was observed for responses recorded from L4 cells (406 ± 166 μs; $n = 12$). Latencies of individual PSPs in pyramidal and MB neurones showed significantly higher scattering (jitter 871 ± 219 μs, $n = 10$ and 833 ± 177 μs, $n = 9$; $P < 0.01$ respectively). The highest synaptic jitter was observed in MCR cells, where individual jitter values ranged from 1100 to 3950 μs, with an average of 2262 ± 912 μs ($n = 9$).

Additional evidence that MB, layer 2/3 pyramidal and MCR neurons receive polysynaptic excitation upon thalamic stimulation stems from the following experiments. AMPA and NMDA mediated EPSCs were recorded in neurons held at −70 mV or +40 mV in presence or absence of the AMPA receptor channel antagonist CNQX (20 μM). Gabazine (10 μM) was added to the bath solution to block inhibition. Cesium-containing intracellular solution was used to improve spatial clamp and EPSCs were evoked by minimal stimulation. After collecting 50 sweeps at −70 and +40 mV, CNQX was applied. In L4 cells NMDA mediated EPSCs were present after CNQX application confirming the monosynaptic nature of thalamic driven EPSCs (Fig. 10*B*). In contrast, in MB, pyramidal and MCR cells, NMDA mediated EPSCs at positive potentials could not be measured in the presence of CNQX. Thus, most probably, MB cells receive direct input from layer 4, whereas MCR cells receive little or no direct input from layer 4, relying on the activation of layer 2/3 pyramidal cells for the relay of thalamic input.

Discussion

GABAergic interneurons have been classified based on a number of criteria, including anatomical, physiological and molecular characteristics (Freund and Buzsaki 1996; Kawaguchi and Kubota 1997; Markram et al. 2004; Monyer and Markram 2004). However, when several criteria were taken into account, it became apparent that there was not always a direct correlation between the variables of one classification with those of another. A multidisciplinary approach to study GABAergic interneurons taking into account anatomical, electrophysiological and molecular criteria resulted in an ever increasing number of subtypes and a controversy as to the meaning and usefulness of a given classification arose (Parra et al. 1998; Yuste 2005). Transgenic mice with EGFP-labeled interneuron subtypes have been an important aid because they allow the efficient systematic study of identified interneurons employing a combination of diverse techniques (Oliva et al. 2000; Meyer et al. 2002; Chattopadhyaya et al. 2004; Ma et al. 2006).

We generated transgenic mice expressing EGFP in CR-positive cells to conduct anatomical studies and to investigate physiological properties of these cells in the neocortex. The expression analysis of the transgene revealed that there was no perfect match of EGFP expression in CR-positive cells. This might result from the EGFP insertion into the CR gene preventing complete temporal and spatial control of the transgene expression allude to the interruption of some regulatory element (e.g., promoter/enhancer sequences; RNA processing regions). It is unlikely that the site of BAC integration contributes to misexpression because a similar pattern and intensity of EGFP expression was found in 2 founders. It is of note that in areas with strong CR expression (e.g., olfactory bulb) there is a high degree of colocalization. Despite of incomplete EGFP labeling, it was possible to identify 2 distinct types of cortical EGFP/CR-positive interneurons.

In this study we focused on layer 2/3 cortical CR-positive cells and compared their features with those of MB and FS cells. In a previous study, we used mice expressing EGFP in parvalbumin-positive cells and identified a new cell type, the MB cell (Blatow et al. 2003). Electrophysiological, anatomical and biochemical features of MB cells differed from those of FS cells, another subclass of parvalbumin-positive interneurons that had been studied quite extensively (Kawaguchi and Kubota 1997; Reyes et al. 1998; Povysheva et al. 2006).

We describe the identification of 2 distinct EGFP/CR-positive cell types: BCR and MCR cells. BCR cells are bipolar, with vertical axonal extensions and have a bursting firing pattern, whereas MCR cells are multipolar, with horizontal neurite extensions and show a regular firing pattern with pronounced adaptation and accommodation. Both cell types most likely correspond to cell types described in previous studies. Thus, cortical CR-positive neurons of bipolar and multipolar shape have been described in different species (Andressen et al. 1993; del Rio and DeFelipe 1997; Defelipe et al. 1999; Gonchar and Burkhalter 2003). CR-positive, VIP-positive, bipolar cells with a bursting AP pattern were found in the rat (Kawaguchi and Kubota 1996; Cauli et al. 1997). Small horizontal multipolar cells (of unknown immunoreactivity) with an adapting firing pattern were identified in rat visual cortex (Dantzker and Callaway 2000).

As in the hippocampus (for review see Freund and Buzsaki 1996) CR-positive cells in the neocortex preferentially innervate other interneurons. These results are also in agreement with previous anatomical studies in rat visual cortex (Gonchar and Burkhalter 1999). In this study the authors reported that the most frequent target of CR-positive terminals were CR-positive dendrites. Our own results corroborated and extended these findings. Thus using paired recordings we established that CR-positive interneurons of one subtype mainly innervate cells belonging to the other subtype. Indeed, BCR cells innervate more frequently MCR cells rather than BCR cells and vice versa. Of particular note in this respect are MCR cells whose preferred target are the MB cells. The fact that these 2 cell types are also connected via gap junctions indicates their special relationship within a microcircuit. In this study we have used sagittal section for one main reason: it allowed us to compare chemical and electrical connectivity with our previous data obtained both in mouse and rat for other interneurons (Reyes et al. 1998; Rozov et al. 2001; Blatow et al. 2003). Although connectivity measure might be underestimated, like in any slice preparation because neurons in slices are incomplete, we still think that this method is reflecting the relative differences of connectivity between different cell types.

Electrical coupling between GABAergic interneurons has been a major focus of several studies demonstrating that gap junction coupling was restricted to GABAergic interneurons of the same subtype (Galarreta and Hestrin 1999, 2001, 2002; Gibson et al. 1999, 2005; Beierlein et al. 2000; Tamas et al. 2000; Venance et al. 2000; Deans et al. 2001; Amitai et al. 2002; Meyer et al. 2002). It appears that selective electrical synapses constitute one way by which coexisting interneuron networks within a microcircuit are delineated (see reviews (Bennett and Zukin 2004; Hestrin and Galarreta 2005). Neurogliaform cells are an exception in this regard because they are connected via gap junctions not only to neurogliaform cells but also to other cell types including FS basket cells, regular spiking non-pyramidal cells and cells that were not, in that study, unambiguously classified, thus bridging interneuronal network separations (Simon et al. 2005). In this study we demonstrate that, whereas BCR cells form gap junctions with other cells of the same kind, MCR cells do not form electrical synapses with other MCR cells, but, of the cell types tested here, only with MB cells. We had previously shown that MB cells form a novel interneuron network that can induce synchronized IPSPs in populations of layer 2/3 pyramidal cells and thereby phase-lock their firing activity (Blatow et al. 2003). This conclusion was supported by the following observations: MB cells frequently innervated pyramidal cells (success rate ~40%); there was a high success rate (96%) of gap junction coupling between MB cells; bath application of carbachol-induced theta frequency oscillations within MB cell network and could drive synchronized inhibition of pyramidal cells. Here we provide evidence that MCR cells are part of this network when they are electrically connected with MB cells. It is of note that MB and MCR cells receive distinct excitatory inputs in the neocortex: the latter seem to be recruited from layer 2/3 pyramidal cells, whereas MB cells might be recruited also from layer 4 excitatory cells. Thus, MB-MCR cell ensembles may play a critical role in shaping cortical oscillations because they are able to integrate excitation coming from different neocortical layers.

Furthermore the different dynamic properties of their synapses are worth emphasizing: the excitatory drive onto MCR cells is facilitating implying an increase in excitability during rhythmic activity, whereas the excitatory input onto MB cells is depressing. One can speculate that MB cells are critically involved in the initiation of theta frequency oscillations whereas MCR cells maintain the rhythmic activity in this network.

BCR cells do not appear to play a role in the MCR-MB cell network under the conditions tested here because they are not responsive to carbachol activation (data not shown). Given that they frequently target other layer 2/3 interneurons, their major role is probably to act as "disinhibitory" cells, relieving layer 2/3 pyramidal cells from inhibition. In summary, using transgenic mice with EGFP-labeled CR-positive neurons, we identified 2 distinct cell types that differ with respect to their morphological, electrophysiological and functional properties.

Supplementary Material

Supplementary material can be found at: http://www.cercor.oxfordjournals.org/

Funding

Schilling Foundation to H.M.; EUSynapse project grant (LSHM-CT-2005-019055); and Development Grant Facility grant (FOR 577/1) to A.R.

Notes

We thank Axel H. Meyer for help with the BAC cloning. *Conflict of Interest*: None declared.

Address correspondence to Hannah Monyer, Department of Clinical Neurobiology, University of Heidelberg, Im Neuenheimer Feld 364, 69120 Heidelberg, Germany. Email: monyer@urz.uni-heidelberg.de.

References

Agmon A, Connors BW. 1991. Thalamocortical responses of mouse somatosensory (barrel) cortex in vitro. Neuroscience. 41:365–379.

Amitai Y, Gibson JR, Beierlein M, Patrick SL, Ho AM, Connors BW, Golomb D. 2002. The spatial dimensions of electrically coupled networks of interneurons in the neocortex. J Neurosci. 22:4142–4152.

Andressen C, Blumcke I, Celio MR. 1993. Calcium-binding proteins: selective markers of nerve cells. Cell Tissue Res. 271:181–208.

Beierlein M, Gibson JR, Connors BW. 2000. A network of electrically coupled interneurons drives synchronized inhibition in neocortex. Nat Neurosci. 3:904–910.

Beierlein M, Gibson JR, Connors BW. 2003. Two dynamically distinct inhibitory networks in layer 4 of the neocortex. J Neurophysiol. 90:2987–3000.

Bennett MV, Zukin RS. 2004. Electrical coupling and neuronal synchronization in the mammalian brain. Neuron. 41:495–511.

Blatow M, Rozov A, Katona I, Hormuzdi SG, Meyer AH, Whittington MA, Caputi A, Monyer H. 2003. A novel network of multipolar bursting interneurons generates theta frequency oscillations in neocortex. Neuron. 38:805–817.

Buhl EH, Tamas G, Fisahn A. 1998. Cholinergic activation and tonic excitation induce persistent gamma oscillations in mouse somatosensory cortex in vitro. J Physiol. 513(Pt 1):117–126.

Cauli B, Audinat E, Lambolez B, Angulo MC, Ropert N, Tsuzuki K, Hestrin S, Rossier J. 1997. Molecular and physiological diversity of cortical nonpyramidal cells. J Neurosci. 17:3894–3906.

Chattopadhyaya B, Di Cristo G, Higashiyama H, Knott GW, Kuhlman SJ, Welker E, Huang ZJ. 2004. Experience and activity-dependent maturation of perisomatic GABAergic innervation in primary visual cortex during a postnatal critical period. J Neurosci. 24:9598–9611.

Chmielowska J, Carvell GE, Simons DJ. 1989. Spatial organization of thalamocortical and corticothalamic projection systems in the rat SmI barrel cortex. J Comp Neurol. 285:325–338.

Cobb SR, Buhl EH, Halasy K, Paulsen O, Somogyi P. 1995. Synchronization of neuronal activity in hippocampus by individual GABAergic interneurons. Nature. 378:75–78.

Cruikshank SJ, Lewis TJ, Connors BW. 2007. Synaptic basis for intense thalamocortical activation of feedforward inhibitory cells in neocortex. Nat Neurosci. 10:462–468.

Cunningham MO, Davies CH, Buhl EH, Kopell N, Whittington MA. 2003. Gamma oscillations induced by kainate receptor activation in the entorhinal cortex in vitro. J Neurosci. 23:9761–9769.

Dantzker JL, Callaway EM. 2000. Laminar sources of synaptic input to cortical inhibitory interneurons and pyramidal neurons. Nat Neurosci. 3:701–707.

Deans MR, Gibson JR, Sellitto C, Connors BW, Paul DL. 2001. Synchronous activity of inhibitory networks in neocortex requires electrical synapses containing connexin36. Neuron. 31:477–485.

DeFelipe J. 1997. Types of neurons, synaptic connections and chemical characteristics of cells immunoreactive for calbindin-D28K, parvalbumin and calretinin in the neocortex. J Chem Neuroanat. 14:1–19.

Defelipe J, Gonzalez-Albo MC, Del Rio MR, Elston GN. 1999. Distribution and patterns of connectivity of interneurons containing calbindin, calretinin, and parvalbumin in visual areas of the occipital and temporal lobes of the macaque monkey. J Comp Neurol. 412:515–526.

del Rio MR, DeFelipe J. 1997. Synaptic connections of calretinin-immunoreactive neurons in the human neocortex. J Neurosci. 17:5143–5154.

Douglas RJ, Martin KA. 2004. Neuronal circuits of the neocortex. Annu Rev Neurosci. 27:419–451.

Doyle MW, Andresen MC. 2001. Reliability of monosynaptic sensory transmission in brain stem neurons in vitro. J Neurophysiol. 85:2213–2223.
Forehand CJ, Konopka LM. 1989. Frog sympathetic ganglion cells have local axon collaterals. J Comp Neurol. 289:294–303.
Freund TF, Buzsaki G. 1996. Interneurons of the hippocampus. Hippocampus. 6:347–470.
Galarreta M, Hestrin S. 1998. Frequency-dependent synaptic depression and the balance of excitation and inhibition in the neocortex. Nat Neurosci. 1:587–594.
Galarreta M, Hestrin S. 1999. A network of fast-spiking cells in the neocortex connected by electrical synapses. Nature. 402:72–75.
Galarreta M, Hestrin S. 2001. Spike transmission and synchrony detection in networks of GABAergic interneurons. Science. 292:2295–2299.
Galarreta M, Hestrin S. 2002. Electrical and chemical synapses among parvalbumin fast-spiking GABAergic interneurons in adult mouse neocortex. Proc Natl Acad Sci USA. 99:12438–12443.
Gibson JR, Beierlein M, Connors BW. 1999. Two networks of electrically coupled inhibitory neurons in neocortex. Nature. 402:75–79.
Gibson JR, Beierlein M, Connors BW. 2005. Functional properties of electrical synapses between inhibitory interneurons of neocortical layer 4. J Neurophysiol. 93:467–480.
Gireesh ED, Plenz D. 2008. Neuronal avalanches organize as nested theta- and beta/gamma-oscillations during development of cortical layer 2/3. Proc Natl Acad Sci USA. 105:7576–7581.
Gonchar Y, Burkhalter A. 1999. Connectivity of GABAergic calretinin-immunoreactive neurons in rat primary visual cortex. Cereb Cortex. 9:683–696.
Gonchar Y, Burkhalter A. 2003. Distinct GABAergic targets of feedforward and feedback connections between lower and higher areas of rat visual cortex. J Neurosci. 23:10904–10912.
Gulyas AI, Hajos N, Freund TF. 1996. Interneurons containing calretinin are specialized to control other interneurons in the rat hippocampus. J Neurosci. 16:3397–3411.
Gupta A, Wang Y, Markram H. 2000. Organizing principles for a diversity of GABAergic interneurons and synapses in the neocortex. Science. 287:273–278.
Hestrin S, Galarreta M. 2005. Electrical synapses define networks of neocortical GABAergic neurons. Trends Neurosci. 28:304–309.
Holmgren C, Harkany T, Svennenfors B, Zilberter Y. 2003. Pyramidal cell communication within local networks in layer 2/3 of rat neocortex. J Physiol. 551:139–153.
Kawaguchi Y, Kubota Y. 1996. Physiological and morphological identification of somatostatin- or vasoactive intestinal polypeptide-containing cells among GABAergic cell subtypes in rat frontal cortex. J Neurosci. 16:2701–2715.
Kawaguchi Y, Kubota Y. 1997. GABAergic cell subtypes and their synaptic connections in rat frontal cortex. Cereb Cortex. 7:476–486.
Koralek KA, Jensen KF, Killackey HP. 1988. Evidence for two complementary patterns of thalamic input to the rat somatosensory cortex. Brain Res. 463:346–351.
Llinas RR, Leznik E, Urbano FJ. 2002. Temporal binding via cortical coincidence detection of specific and nonspecific thalamocortical inputs: a voltage-dependent dye-imaging study in mouse brain slices. Proc Natl Acad Sci USA. 99:449–454.
Lu SM, Lin RC. 1993. Thalamic afferents of the rat barrel cortex: a light- and electron-microscopic study using Phaseolus vulgaris leucoagglutinin as an anterograde tracer. Somatosens Mot Res. 10:1–16.
Lubke J, Feldmeyer D. 2007. Excitatory signal flow and connectivity in a cortical column: focus on barrel cortex. Brain Struct Funct. 212:3–17.
Ma Y, Hu H, Berrebi AS, Mathers PH, Agmon A. 2006. Distinct subtypes of somatostatin-containing neocortical interneurons revealed in transgenic mice. J Neurosci. 26:5069–5082.
Markram H, Lubke J, Frotscher M, Roth A, Sakmann B. 1997. Physiology and anatomy of synaptic connections between thick tufted pyramidal neurones in the developing rat neocortex. J Physiol. 500(Pt 2):409–440.
Markram H, Toledo-Rodriguez M, Wang Y, Gupta A, Silberberg G, Wu C. 2004. Interneurons of the neocortical inhibitory system. Nat Rev Neurosci. 5:793–807.
McBain CJ, Fisahn A. 2001. Interneurons unbound. Nat Rev Neurosci. 2:11–23.
Meyer AH, Katona I, Blatow M, Rozov A, Monyer H. 2002. In vivo labeling of parvalbumin-positive interneurons and analysis of electrical coupling in identified neurons. J Neurosci. 22:7055–7064.
Monyer H, Markram H. 2004. Interneuron diversity series: molecular and genetic tools to study GABAergic interneuron diversity and function. Trends Neurosci. 27:90–97.
Oliva AA, Jr, Jiang M, Lam T, Smith KL, Swann JW. 2000. Novel hippocampal interneuronal subtypes identified using transgenic mice that express green fluorescent protein in GABAergic interneurons. J Neurosci. 20:3354–3368.
Parra P, Gulyas AI, Miles R. 1998. How many subtypes of inhibitory cells in the hippocampus? Neuron. 20:983–993.
Povysheva NV, Gonzalez-Burgos G, Zaitsev AV, Kroner S, Barrionuevo G, Lewis DA, Krimer LS. 2006. Properties of excitatory synaptic responses in fast-spiking interneurons and pyramidal cells from monkey and rat prefrontal cortex. Cereb Cortex. 16:541–552.
Price CJ, Cauli B, Kovacs ER, Kulik A, Lambolez B, Shigemoto R, Capogna M. 2005. Neurogliaform neurons form a novel inhibitory network in the hippocampal CA1 area. J Neurosci. 25:6775–6786.
Reyes A, Lujan R, Rozov A, Burnashev N, Somogyi P, Sakmann B. 1998. Target-cell-specific facilitation and depression in neocortical circuits. Nat Neurosci. 1:279–285.
Roopun AK, Middleton SJ, Cunningham MO, LeBeau FE, Bibbig A, Whittington MA, Traub RD. 2006. A beta2-frequency (20-30 Hz) oscillation in nonsynaptic networks of somatosensory cortex. Proc Natl Acad Sci USA. 103:15646–15650.
Rozov A, Jerecic J, Sakmann B, Burnashev N. 2001. AMPA receptor channels with long-lasting desensitization in bipolar interneurons contribute to synaptic depression in a novel feedback circuit in layer 2/3 of rat neocortex. J Neurosci. 21:8062–8071.
Simon A, Olah S, Molnar G, Szabadics J, Tamas G. 2005. Gap-junctional coupling between neurogliaform cells and various interneuron types in the neocortex. J Neurosci. 25:6278–6285.
Somogyi P, Klausberger T. 2005. Defined types of cortical interneurone structure space and spike timing in the hippocampus. J Physiol. 562:9–26.
Tamas G, Buhl EH, Lorincz A, Somogyi P. 2000. Proximally targeted GABAergic synapses and gap junctions synchronize cortical interneurons. Nat Neurosci. 3:366–371.
Tan Z, Hu H, Huang ZJ, Agmon A. 2008. Robust but delayed thalamocortical activation of dendritic-targeting inhibitory interneurons. Proc Natl Acad Sci USA. 105:2187–2192.
Venance L, Rozov A, Blatow M, Burnashev N, Feldmeyer D, Monyer H. 2000. Connexin expression in electrically coupled postnatal rat brain neurons. Proc Natl Acad Sci USA. 97:10260–10265.
Wang Y, Gupta A, Toledo-Rodriguez M, Wu CZ, Markram H. 2002. Anatomical, physiological, molecular and circuit properties of nest basket cells in the developing somatosensory cortex. Cereb Cortex. 12:395–410.
Whittington MA, Traub RD, Jefferys JG. 1995. Synchronized oscillations in interneuron networks driven by metabotropic glutamate receptor activation. Nature. 373:612–615.
Ylinen A, Bragin A, Nadasdy Z, Jando G, Szabo I, Sik A, Buzsaki G. 1995. Sharp wave-associated high-frequency oscillation (200 Hz) in the intact hippocampus: network and intracellular mechanisms. J Neurosci. 15:30–46.
Ylinen A, Soltesz I, Bragin A, Penttonen M, Sik A, Buzsaki G. 1995. Intracellular correlates of hippocampal theta rhythm in identified pyramidal cells, granule cells, and basket cells. Hippocampus. 5:78–90.
Yuste R. 2005. Origin and classification of neocortical interneurons. Neuron. 48:524–527.